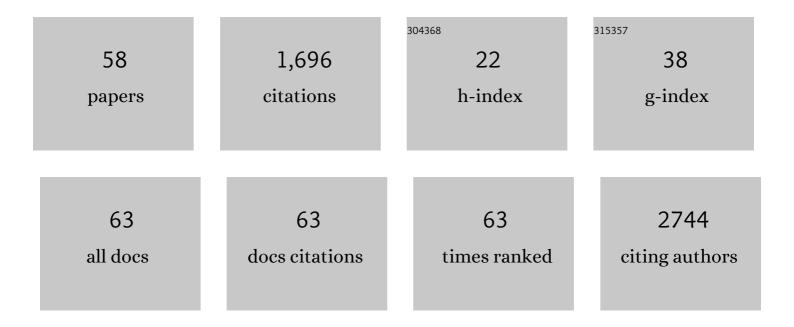
Stephan Block

List of Publications by Year in descending order

Source: https://exaly.com/author-pdf/3806808/publications.pdf Version: 2024-02-01



STEDHAN RIOCK

#	Article	IF	CITATIONS
1	Heteromultivalent topology-matched nanostructures as potent and broad-spectrum influenza A virus inhibitors. Science Advances, 2021, 7, .	4.7	25
2	Particle Diffusivity and Free-Energy Profiles in Hydrogels from Time-Resolved Penetration Data. Biophysical Journal, 2021, 120, 463-475.	0.2	12
3	Automated Solventâ€Free Polymerization of Hyperbranched Polyglycerol with Tailored Molecular Weight by Online Torque Detection. Macromolecular Materials and Engineering, 2021, 306, 2000688.	1.7	11
4	Wrapping and Blocking of Influenza A Viruses by Sialylated 2D Nanoplatforms. Advanced Materials Interfaces, 2021, 8, 2100285.	1.9	17
5	Polysulfate hemmen durch elektrostatische Wechselwirkungen die SARSâ€CoVâ€2â€Infektion**. Angewandte Chemie, 2021, 133, 16005-16014.	1.6	0
6	Polysulfates Block SARSâ€CoVâ€2 Uptake through Electrostatic Interactions**. Angewandte Chemie - International Edition, 2021, 60, 15870-15878.	7.2	49
7	Physiological Shear Stress Enhances Differentiation, Mucus-Formation and Structural 3D Organization of Intestinal Epithelial Cells In Vitro. Cells, 2021, 10, 2062.	1.8	17
8	Physicochemical tools for studying virus interactions with targeted cell membranes in a molecular and spatiotemporally resolved context. Analytical and Bioanalytical Chemistry, 2021, 413, 7157-7178.	1.9	11
9	One-pot gram-scale synthesis of virucidal heparin-mimicking polymers as HSV-1 inhibitors. Chemical Communications, 2021, 57, 11948-11951.	2.2	12
10	Lipid Composition Affects the Efficiency in the Functional Reconstitution of the Cytochrome c Oxidase. International Journal of Molecular Sciences, 2020, 21, 6981.	1.8	5
11	Mucinâ€Inspired, High Molecular Weight Virus Binding Inhibitors Show Biphasic Binding Behavior to Influenza A Viruses. Small, 2020, 16, e2004635.	5.2	15
12	Directed manipulation of membrane proteins by fluorescent magnetic nanoparticles. Nature Communications, 2020, 11, 4259.	5.8	27
13	Independent Size and Fluorescence Emission Determination of Individual Biological Nanoparticles Reveals that Lipophilic Dye Incorporation Does Not Scale with Particle Size. Langmuir, 2020, 36, 9693-9700.	1.6	6
14	Adaptive Flexible Sialylated Nanogels as Highly Potent Influenza A Virus Inhibitors. Angewandte Chemie, 2020, 132, 12517-12522.	1.6	5
15	Analysis and refinement of 2D single-particle tracking experiments. Biointerphases, 2020, 15, 021201.	0.6	11
16	Directed Manipulation of Membrane Proteins by Fluorescent Magnetic Nanoparticles. Biophysical Journal, 2020, 118, 313a.	0.2	3
17	Adaptive Flexible Sialylated Nanogels as Highly Potent Influenza A Virus Inhibitors. Angewandte Chemie - International Edition, 2020, 59, 12417-12422.	7.2	36
18	Competition for Membrane Receptors: Norovirus Detachment via Lectin Attachment. Journal of the American Chemical Society, 2019, 141, 16303-16311.	6.6	18

STEPHAN BLOCK

#	Article	IF	CITATIONS
19	Mobility-Based Quantification of Multivalent Virus-Receptor Interactions: New Insights Into Influenza A Virus Binding Mode. Nano Letters, 2019, 19, 1875-1882.	4.5	60
20	Membrane Deformation Induces Clustering of Norovirus Bound to Glycosphingolipids in a Supported Cell-Membrane Mimic. Journal of Physical Chemistry Letters, 2018, 9, 2278-2284.	2.1	12
21	Cell Membrane Derived Platform To Study Virus Binding Kinetics and Diffusion with Single Particle Sensitivity. ACS Infectious Diseases, 2018, 4, 944-953.	1.8	24
22	Antenna-Enhanced Fluorescence Correlation Spectroscopy Resolves Calcium-Mediated Lipid–Lipid Interactions. ACS Nano, 2018, 12, 3272-3279.	7.3	3
23	Affinity Purification and Single-Molecule Analysis of Integral Membrane Proteins from Crude Cell-Membrane Preparations. Nano Letters, 2018, 18, 381-385.	4.5	12
24	MicroRNA Detection by DNAâ€Mediated Liposome Fusion. ChemBioChem, 2018, 19, 434-438.	1.3	35
25	Brownian Motion at Lipid Membranes: A Comparison of Hydrodynamic Models Describing and Experiments Quantifying Diffusion within Lipid Bilayers. Biomolecules, 2018, 8, 30.	1.8	20
26	Stable 2D Conductive Ga/Ga(O <i>_x</i> H <i>_y</i>) Multilayers with Controlled Nanoscale Thickness Prepared from Gallium Droplets with Oxide Skin. Advanced Materials Interfaces, 2018, 5, 1800323.	1.9	9
27	Effective Refractive Index and Lipid Content of Extracellular Vesicles Revealed Using Optical Waveguide Scattering and Fluorescence Microscopy. Langmuir, 2018, 34, 8522-8531.	1.6	22
28	A nano flow cytometer for single lipid vesicle analysis. Lab on A Chip, 2017, 17, 830-841.	3.1	66
29	Single Proteoliposomes with <i>E.Âcoli</i> Quinol Oxidase: Proton Pumping without Transmembrane Leaks. Israel Journal of Chemistry, 2017, 57, 437-445.	1.0	11
30	Detachment of Membrane Bound Virions by Competitive Ligand Binding Induced Receptor Depletion. Langmuir, 2017, 33, 4049-4056.	1.6	18
31	Binding Kinetics and Lateral Mobility of HSV-1 on End-Grafted Sulfated Glycosaminoglycans. Biophysical Journal, 2017, 113, 1223-1234.	0.2	27
32	Hydrodynamic Propulsion of Liposomes Electrostatically Attracted to a Lipid Membrane Reveals Size-Dependent Conformational Changes. ACS Nano, 2016, 10, 8812-8820.	7.3	12
33	Dual-Wavelength Surface Plasmon Resonance for Determining the Size and Concentration of Sub-Populations of Extracellular Vesicles. Analytical Chemistry, 2016, 88, 9980-9988.	3.2	70
34	Two-dimensional flow nanometry of biological nanoparticles for accurate determination of their size and emission intensity. Nature Communications, 2016, 7, 12956.	5.8	34
35	Quantification of Multivalent Interactions by Tracking Single Biological Nanoparticle Mobility on a Lipid Membrane. Nano Letters, 2016, 16, 4382-4390.	4.5	58
36	Imaging and Characterization of Magnetic Micro- and Nanostructures Using Force Microscopy. , 2015, , 489-529.		0

STEPHAN BLOCK

#	Article	IF	CITATIONS
37	Morphology, Mechanical Stability, and Protective Properties of Ultrathin Gallium Oxide Coatings. Langmuir, 2015, 31, 5836-5842.	1.6	20
38	Sequence-controlled RNA self-processing: computational design, biochemical analysis, and visualization by AFM. Rna, 2015, 21, 1249-1260.	1.6	18
39	AFM-Based Quantification of Conformational Changes in DNA Caused by Reactive Oxygen Species. Journal of Physical Chemistry B, 2015, 119, 25-32.	1.2	13
40	Characterisation of the conformational changes in platelet factor 4 induced by polyanions: towards in vitro prediction of antigenicity. Thrombosis and Haemostasis, 2014, 112, 53-64.	1.8	67
41	Determination of Exosome Concentration in Solution Using Surface Plasmon Resonance Spectroscopy. Analytical Chemistry, 2014, 86, 5929-5936.	3.2	133
42	Characterization of bonds formed between platelet factor 4 and negatively charged drugs using single molecule force spectroscopy. Soft Matter, 2014, 10, 2775.	1.2	15
43	Stiffness of Left Ventricular Cardiac Fibroblasts Is Associated With Ventricular Dilation in Patients With Recent-Onset Nonischemic and Nonvalvular Cardiomyopathy. Circulation Journal, 2014, 78, 1693-1700.	0.7	9
44	Binding of anti–platelet factor 4/heparin antibodies depends on the thermodynamics of conformational changes in platelet factor 4. Blood, 2014, 124, 2442-2449.	0.6	67
45	Effects of Reactive Oxygen Species on Single Polycation Layers. Journal of Physical Chemistry B, 2013, 117, 8475-8483.	1.2	4
46	Complex formation with nucleic acids and aptamers alters the antigenic properties of platelet factor 4. Blood, 2013, 122, 272-281.	0.6	129
47	Temperature-Induced Transition from Odd–Even to Even–Odd Effect in Polyelectrolyte Multilayers Due to Interpolyelectrolyte Interactions. Journal of Physical Chemistry B, 2012, 116, 1234-1243.	1.2	27
48	Equilibrium and Nonequilibrium Features in the Morphology and Structure of Physisorbed Polyelectrolyte Layers. Journal of Physical Chemistry B, 2011, 115, 7301-7313.	1.2	15
49	Direct Visualization and Identification of Biofunctionalized Nanoparticles using a Magnetic Atomic Force Microscope. Nano Letters, 2011, 11, 3587-3592.	4.5	18
50	Size-controlled formation of Cu nanoclusters in pulsed magnetron sputtering system. Surface and Coatings Technology, 2011, 205, 2755-2762.	2.2	57
51	Effect of 3D-scaffold formation on differentiation and survival in human neural progenitor cells. BioMedical Engineering OnLine, 2010, 9, 70.	1.3	71
52	Destabilization of Polyelectrolyte Multilayers Formed at Different Temperatures and Ion Concentrations. Macromolecules, 2010, 43, 4300-4309.	2.2	26
53	Single Polyelectrolyte Layers Adsorbed at High Salt Conditions: Polyelectrolyte Brush Domains Coexisting with Flatly Adsorbed Chains. Macromolecules, 2009, 42, 6733-6740.	2.2	25
54	Physical properties of homogeneous TiO ₂ films prepared by high power impulse magnetron sputtering as a function of crystallographic phase and nanostructure. Journal Physics D: Applied Physics, 2009, 42, 105204.	1.3	52

STEPHAN BLOCK

#	Article	IF	CITATIONS
55	The adhesion and spreading of thrombocyte vesicles on electrode surfaces. Bioelectrochemistry, 2008, 74, 210-216.	2.4	25
56	Conformation of Poly(styrene sulfonate) Layers Physisorbed from High Salt Solution Studied by Force Measurements on Two Different Length Scales. Journal of Physical Chemistry B, 2008, 112, 9318-9327.nt of long-ranged steric forces between polyelectrolyte layers physisorbed	1.2	56
57	from <mmi:math_xmins:mmi="http: 1998="" math="" math<="" td="" www.w3.org=""><td>0.8</td><td>38</td></mmi:math_xmins:mmi="http:>	0.8	38
58	Semiconductor laser with external resonant grating mirror. IEEE Journal of Quantum Electronics, 2005, 41, 1049-1053.	1.0	31